Inorganic Chemistry

pubs.acs.org/IC

Article

Anisotropic Thermal Expansion and a Second-Order Charge Order Transition in the Ferrimagnetic $Dy_2CuZnMn_4O_{12}$ Perovskite with Triple A-Site Cation Ordering

Alexei A. Belik*

Cite This: *Inorg. Chem.* 2023, 62, 20042−20049

Read Online

ACCESS | Metrics & More | Article Recommendations | Supporting Information

ABSTRACT: $Dy_2CuZnMn_4O_{12}$ perovskite, belonging to the A-site columnar-ordered quadruple perovskite family with the general composition of $A_2A'A''B_4O_{12}$, was prepared by a high-pressure, high-temperature method at 6 GPa and 1500 K. Its crystal structure was studied by synchrotron powder X-ray diffraction between 100 and 800 K. The ideal cation distribution (without antisite disorder) was found to be realized within the sensitivity of the synchrotron X-ray diffraction method. Between 100 and 400 K, it crystallizes in space group *Pmmn* (no. 59) and has layered charge ordering of Mn^{3+} and Mn^{4+} at the B sites. Above 425 K, it crystallizes in space group $P4_2/nmc$ (no. 137) with one crystallographic B site and an average $Mn^{3.5+}$ oxidation state. The charge ordering transition (at T_{CO} = 425 K) appears to be of the second order as no anomalies were found on differential scanning calorimetry curves and temperature dependence of the unit cell volume, and the orthorhombic *a* and *b* lattice parameters merge gradually. The compound demonstrates anisotropic thermal expansion with the *c* lattice parameter decreasing with increasing temperature above 280 K. A ferrimagnetic transition occurs at T_C = 116 K with an additional, gradual rise of magnetic susceptibilities below 45 K, probably due to increases of the ordered moments of the Dy sublattices.

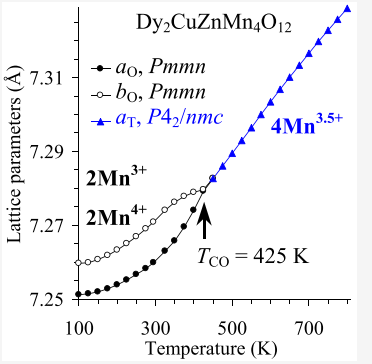

1. INTRODUCTION

A-site columnar-ordered quadruple perovskite oxides with the general composition of $A_2A'A''B_4O_{12}$ are a new playground in the perovskite science to play with compositional variations and their effects on physical properties.[1] In comparison with classical ABO_3 perovskites with one type of A sites and A-site-ordered quadruple perovskites, $AA'_3B_4O_{12}$, with intrinsically two types of A sites (A with a 12-fold coordination and A′ with a square-planar coordination), $A_2A'A''B_4O_{12}$ perovskites have an additional degree of freedom in the presence of the A″ site with a tetrahedral coordination (as the first coordination sphere). Therefore, a principally different, new set of cations, which are not usually located at A sites of perovskites, can be used for the A′′ site, such as Ga^{3+} and Zn^{2+}.[2−5]

The parent structure of the $A_2A'A''B_4O_{12}$ perovskites has $P4_2/nmc$ symmetry and is formed through large tilts of the $a^+a^+c^-$ type.[1] This symmetry is retained in the majority of examples of such perovskites.[1,6] The next most commonly observed symmetry is $P4_2/n$, which is produced through full or partial rock-salt-type B-cation orderings, $A_2A'A''B_2B'_2O_{12}$.[1,6] The less common symmetries are $P4_2mc$ (which is formed through polar distortions in $CaMnTi_2O_6$,[7] $CaMnTi_{2-x}V_xO_6$,[8] and $NaYMnMnTi_4O_{12}$)[9] and *Pmmn* (which is formed through layered-type B-cation ordering in RMn_3O_6 (R = Gd to Tm)[10,11] and $R_2CuMnMn_4O_{12}$ (R = Dy and Y)[12] due to partial or full charge ordering of Mn^{3+} and Mn^{4+}, respectively). The presence of charge-ordered structures based on the same element could suggest the existence of temperature-driven charge-(dis)ordered transitions as observed in simple perovskites (e.g., half-doped $R^{3+}_{0.5}A^{2+}_{0.5}MnO_3$)[13] or quadruple perovskites (e.g., $ACu_3Fe_4O_{12}$).[14] However, such charge-order transitions have not been observed so far in $A_2A'A''B_4O_{12}$ perovskites.[1,10]

In this work, we prepared a new member of the A-site columnar-ordered quadruple perovskite family with the composition of $Dy_2CuZnMn_4O_{12}$. In this compound, a new combination of the A/A′/A″ cations was used ($R^{3+}/Cu^{2+}/Zn^{2+}$) to achieve the triple A-site cation ordering. This combination also gives an average oxidation state of Mn as +3.5—an ideal value for the realization of possible charge ordering. We indeed found that $Dy_2CuZnMn_4O_{12}$ crystallizes in space group *Pmmn* at room temperature with 1:1 charge order of Mn^{3+} and Mn^{4+} at the B sites. High-temperature structural studies showed the existence of a charge-disorder transition above 425 K, which is of the second order. We also observed anisotropic thermal expansion above 280 K and a ferrimagnetic transition below T_C = 116 K.

Received: August 15, 2023
Revised: October 20, 2023
Accepted: November 8, 2023
Published: November 27, 2023

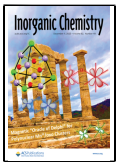

https://doi.org/10.1021/acs.inorgchem.3c02835
Inorg. Chem. 2023, 62, 20042−20049

2. EXPERIMENTAL SECTION

$Dy_2CuZnMn_4O_{12}$ was prepared from a stoichiometric mixture of *o*-$DyMnO_3$, ZnO (99.9%), CuO (99.9%), and MnO_2 (Alfa Aesar, 99.9%) at about 6 GPa and about 1500 K for 2 h in Au capsules. After annealing at 1500 K, the samples were cooled down to room temperature by turning off the heating current, and the pressure was slowly released. We note that the oxygen content of a commercial well-crystallized single-phase MnO_2 chemical was confirmed by thermal analysis. Single-phase *o*-$DyMnO_3$ was prepared from a stoichiometric mixture of Dy_2O_3 (99.9%) and Mn_2O_3 (99.99%) by annealing in air at 1430 K for 60 h with several intermediate grindings. After the high-pressure synthesis, the sample was recovered as black powder (Figure S1). Therefore, some measurements (such as, specific heat, resistivity, and dielectric constant), which require dense pellets, could not be performed. We note that the melting point of Au at 6 GPa is above 1600 K;[15] therefore, Au capsules could be safely used for the synthesis at 1500 K. We did not observe any reaction between Au and $Dy_2CuZnMn_4O_{12}$ or any damage of Au capsules.

X-ray powder diffraction (XRPD) data were collected at room temperature on a RIGAKU MiniFlex600 diffractometer using Cu Kα radiation (2θ range of 8−100°, a step width of 0.02°, and scan speed of 2°/min). Synchrotron XRPD data were collected from 100 to 800 K on beamline BL02B2 of SPring-8 (the intensity data were taken between 2.08° and 78.22° at 0.006° intervals in 2θ using a wavelength of λ = 0.619283 Å).[16] High statistics data with a measurement time of 100 s were collected at 100, 295, and 600 K; at all other temperatures, the measurement time was 10 s. The sample was placed into an open Lindemann glass capillary tube (inner diameter: 0.2 mm), which was rotated during measurements. The Rietveld analysis of all XRPD data was performed using the *RIETAN-2000* program.[17]

Magnetic measurements were performed on a SQUID magnetometer (Quantum Design, MPMS3) between 2 and 400 K in applied fields of 100 Oe and 10 kOe under both zero-field-cooled (ZFC) and field-cooled on cooling (FCC) conditions. High-temperature data were taken at 70 kOe from 300 to 470 K. Isothermal magnetization measurements were performed between −70 and 70 kOe at different temperatures. A small sample weight of 11.09 mg was used for the dc magnetic measurements because of a large magnetic moment (1.82 emu at 5 K and 70 kOe). Frequency dependent alternating current (ac) susceptibility measurements were performed using a Quantum Design MPMS3 instrument at a zero static dc field and at different frequencies (f) and different applied oscillating magnetic fields (H_{ac}) from 140 to 2 K using a 24.7 mg sample.

Differential scanning calorimetry (DSC) curves of a powder sample were recorded on a Mettler Toledo DSC1 STAR^e system under a N_2 flow between 125 and 670 K in an open Al capsule with a heating/cooling rate of 10 K/min. Two DSC runs were performed to check the reproducibility. No DSC anomalies were found between 125 and 670 K.

3. RESULTS AND DISCUSSION

$Dy_2CuZnMn_4O_{12}$ was found to be single-phase within the sensitivity of the laboratory XRPD data. All its reflections could be indexed in orthorhombic symmetry with a = 7.2599 Å, b = 7.2709 Å, and c = 7.7736 Å. Therefore, the *Pmmn* structural model and the structural parameters of $DyMn_3O_6$ (as the initial ones)[10] were used in the Rietveld analysis of $Dy_2CuZnMn_4O_{12}$. Cu^{2+} (27 electrons) and Zn^{2+} (28 electrons) cations cannot be distinguished by (nonresonant) synchrotron XRPD. Therefore, we assumed the distribution of Cu^{2+} and Zn^{2+} based on their coordination preferences: Zn^{2+} cations have a strong preference for tetrahedral sites (among tetrahedral and square-planar ones) while Cu^{2+} cations have a strong preference for square-planar sites.[18] We note that $CaZnV_2O_6$[19] and $CaCuFeReO_6$[20] were recently prepared, where Zn^{2+} and Cu^{2+} cations are located in both square-planar (A′) and tetrahedral (A″) sites. However, these compounds were stabilized at much higher pressures of 12 and 15.5 GPa, respectively, and they were not stable at 6 GPa. Therefore, we can assume that usual tendencies in the site

Table 1. Structure Parameters of $Dy_2CuZnMn_4O_{12}$ at 100 K (the First Line for Each Site) and 295 K (the Second Line for Each Site) from Synchrotron XRPD Data[a]

site	WP	x	y	z	B_{iso} (Å^2)
Dy1	2*a*	0.25	0.25	0.7785(2)	0.08(2)
		0.25	0.25	0.7784(2)	0.27(3)
Dy2	2*a*	0.25	0.25	0.2786(2)	0.15(3)
		0.25	0.25	0.2786(2)	0.40(3)
Cu	2*b*	0.75	0.25	0.7349(4)	0.41(5)
		0.75	0.25	0.7374(5)	0.61(6)
Zn	2*b*	0.75	0.25	0.2486(4)	0.03(3)
		0.75	0.25	0.2488(5)	0.30(5)
Mn1	4*c*	0.5	0	0	0.03(5)
		0.5	0	0	0.11(8)
Mn2	4*d*	0	0.5	0.5	0.10(5)
		0	0.5	0.5	0.26(8)
O1	8*g*	0.4402(7)	−0.0599(7)	0.2624(10)	0.61(8)
		0.4389(8)	−0.0589(8)	0.2610(11)	1.02(9)
O2	4*f*	0.0634(10)	0.25	0.0336(13)	0.19(12)
		0.0623(10)	0.25	0.0344(13)	0.08(11)
O3	4*e*	0.25	0.5396(11)	0.9105(11)	0.18(13)
		0.25	0.5380(11)	0.9083(12)	0.30(14)
O4	4*f*	0.5391(12)	0.25	0.4231(13)	0.61(16)
		0.5389(11)	0.25	0.4238(13)	0.71(16)
O5	4*e*	0.25	0.4330(10)	0.5386(13)	0.06(11)
		0.25	0.4353(10)	0.5405(13)	0.25(13)

[a]Source: Synchrotron powder X-ray diffraction (λ = 0.61928 Å); used d-space range: from 0.4916 to 7.1 Å. Crystal system: orthorhombic; space group *Pmmn* (no. 59, origin choice 2); Z = 2. Molecular weight: 865.6708 g/mol. The occupation factors (g) of all the sites are unity (g = 1). WP: Wyckoff position. No detectable impurities. 100 K: a = 7.25134(2) Å, b = 7.25958(2) Å, c = 7.76916(1) Å, and V = 408.9820(14) Å^3; R_{wp} = 7.02%, R_p = 5.15%, R_B = 2.86%, and R_F = 1.41%; ρ_{cal} = 7.030 g/cm^3. 295 K: a = 7.25988(2) Å, b = 7.27087(2) Å, c = 7.77362(2) Å, and V = 410.3355(19) Å^3; R_{wp} = 7.26%, R_p = 5.33%, R_B = 3.22%, and R_F = 1.66%; ρ_{cal} = 7.006 g/cm^3.

Table 2. Selected Bond Lengths (l (Å) < 2.8 Å), Bond Angles (deg), Bond Valence Sums, BVS, and Distortion Parameters of MnO_6, Δ, in $Dy_2CuZnMn_4O_{12}$ at 295 K[a]

Dy1−O5 × 2	2.288(9)	Dy2−O2 × 2	2.337(9)
Dy1−O3 × 2	2.325(8)	Dy2−O4 × 2	2.382(9)
Dy1−O2 × 2	2.412(9)	Dy2−O5 × 2	2.441(9)
Dy1−O1 × 4	2.669(7)	Dy2−O1 × 4	2.635(7)
BVS($Dy1^{3+}$)	+3.38	BVS($Dy2^{3+}$)	+3.13
Cu−O1 × 4	1.952(4)	Zn−O3 × 2	1.967(9)
BVS(Cu^{2+})	+1.91	Zn−O4 × 2	2.050(9)
		BVS(Zn^{2+})	+1.77
Mn1−O2 × 2	1.892(2)	Mn2−O5 × 2	1.901(2)
Mn1−O3 × 2	1.969(3)	Mn2−O4 × 2	1.932(3)
Mn1−O1 × 2	2.120(8)	Mn2−O1 × 2	1.958(8)
BVS($Mn1^{3+}$)	+3.29	BVS($Mn2^{4+}$)	+3.72
Δ(Mn1−O)	22.6 × 10^{-4}	Δ(Mn2−O)	1.4 × 10^{-4}
Mn1−O1−Mn2 × 2	144.73(9)	Mn2−O4−Mn2	140.32(9)
Mn1−O2−Mn1	147.75(9)	Mn2−O5−Mn2	145.35(9)
Mn1−O3−Mn1	134.33(9)		

[a]BVS = $\sum_{i=1}^{N} \nu_i$, $\nu_i = \exp[(R_0 - l_i)/B]$, N is the coordination number, B = 0.37, $R_0(Dy^{3+})$ = 2.036, $R_0(Cu^{2+})$ = 1.679, $R_0(Zn^{2+})$ = 1.704, $R_0(Mn^{4+})$ = 1.753, and $R_0(Mn^{3+})$ = 1.76.

https://doi.org/10.1021/acs.inorgchem.3c02835
Inorg. Chem. 2023, 62, 20042−20049

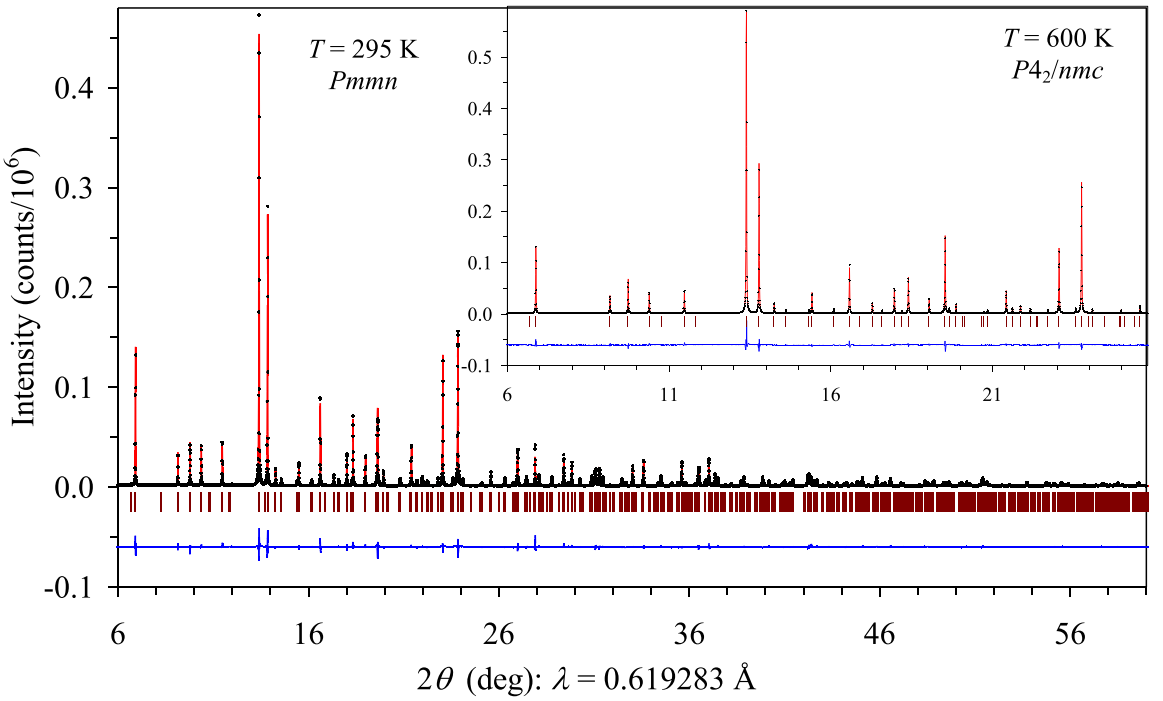

Figure 1. Experimental (black crosses), calculated (red line), and difference (blue line at the bottom) synchrotron powder X-ray diffraction patterns of $Dy_2CuZnMn_4O_{12}$ at T = 295 K between 6 and 60°. The tick marks show possible Bragg reflection positions. The inset shows similar curves at T = 600 K between 6 and 26°.

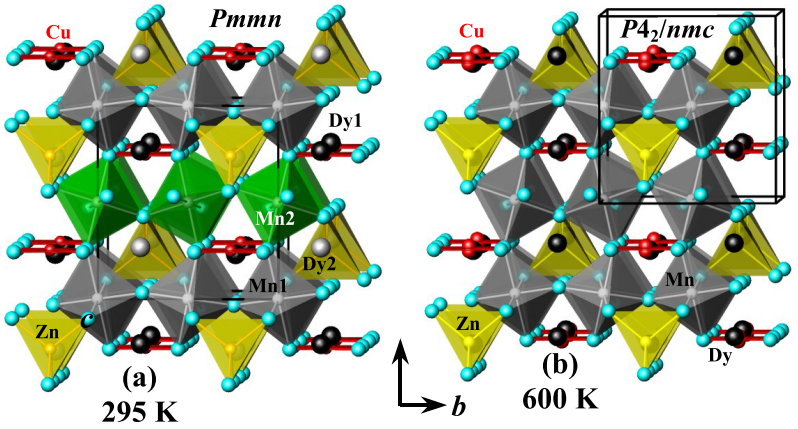

Figure 2. Crystal structures of $Dy_2CuZnMn_4O_{12}$ at (a) T = 295 K in the charge-ordered state and (b) T = 600 K in the charge-disordered state.

preferences for Cu^{2+} and Zn^{2+} cations are realized in $Dy_2CuZnMn_4O_{12}$ prepared at 6 GPa.

Small antisite disorders are often realized in $A_2A'A''B_4O_{12}$ perovskites with A = rare earths, A′ = Mn, and A″ = Mn. Such antisite disorders could be observed with synchrotron XRPD data as small (but detectable) deviations of occupation factors from unity (for ideal cation distribution models).[3−5,11] However, during the structural analysis of $Dy_2CuZnMn_4O_{12}$, all cation occupation factors converged to values close to unity. We report here the occupation factors at 600 K as the symmetry at 600 K is higher (see below) and the number of refined structural parameters is smaller. The following values were obtained (when all other structural and nonstructural parameters were refined simultaneously including atomic displacement parameters): g(Dy) = 0.985(2), g(Cu) = 0.482(3) (for a disordered model with the ideal g = 0.5), and g(Zn) = 0.995(6) with fixed g(Mn) = 1 and g(Cu) = 0.487(3), g(Zn) = 1.014(6), and g(Mn) = 1.018(2) with fixed g(Dy) = 1. We also note that when Mn was located at the tetrahedral A″ site (or the square-planar A′ site), its occupation factor was refined to be 1.265(7) (or 0.600(3) for the A′ site), that is, significantly larger than unity (or 0.5). Therefore, we concluded that the ideal cation distributions are realized in $Dy_2CuZnMn_4O_{12}$ within the sensitivity of synchrotron XRPD data.

Refined structural parameters, primary bond lengths, and bond valence sums (BVS)[21] of $Dy_2CuZnMn_4O_{12}$ at 100 and 295 K are summarized in Tables 1 and 2 and Table S1. Experimental, calculated, and difference synchrotron XRPD patterns of $Dy_2CuZnMn_4O_{12}$ at 295 K are shown in Figure 1. The crystal structure of $Dy_2CuZnMn_4O_{12}$ at 295 K is presented in Figure 2a.

The *Pmmn* structural model was used to obtain the lattice parameters between 100 and 450 K (Figure 3). At 425 and 450

https://doi.org/10.1021/acs.inorgchem.3c02835
Inorg. Chem. 2023, 62, 20042−20049

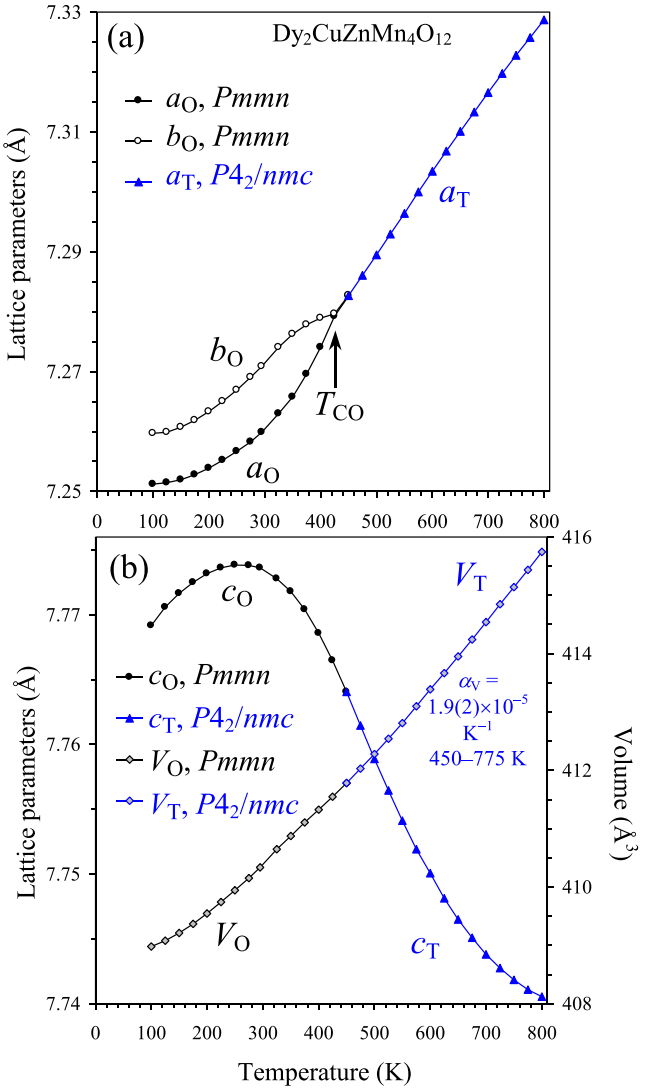

Figure 3. (a) Temperature dependence of the a_O, b_O, and a_T lattice parameters of $Dy_2CuZnMn_4O_{12}$ between 100 and 800 K. (b) Temperature dependence of the c_O and c_T lattice parameters (the left-hand axis) and the unit-cell volume (the right-hand axis) of $Dy_2CuZnMn_4O_{12}$. Errors are smaller than the symbol sizes. α_V is the volumetric coefficient of thermal expansion calculated between T = 450 K and T = 775 K. O, orthorhombic; T, tetragonal.

K, the orthorhombic a_O and b_O lattice parameters already merged, suggesting a phase transition to a tetragonal structure. The orthorhombic splitting of reflections also disappeared (Figure 4). Therefore, at 450 K and above, we used the $P4_2/nmc$ model[3] to obtain temperature dependence of the lattice parameters. The refined structural parameters and bond lengths at 600 K are summarized in Tables 3 and 4, and the fitting patterns are shown in the inset of Figure 1. The crystal structure of $Dy_2CuZnMn_4O_{12}$ at 600 K is given in Figure 2b. We note that the Cu site could be split from the 2*a* site (with g = 1) to the 4*c* site (with g = 0.5) in the $P4_2/nmc$ model.

In the *Pmmn* model, there are two independent sites for the B cations, Mn1 (4*c*) and Mn2 (4*d*). The Mn1 and Mn2 sites have different BVS parameters of +3.29 and +3.72. More importantly, the Mn1 and Mn2 sites have very different octahedral distortion parameters of 22.6 × 10^{-4} and 1.4 × 10^{-4}, respectively. These two facts give evidence that the Mn1 site should be occupied by Mn^{3+} cations resulting in a strong Jahn−Teller distortion of the $Mn1O_6$ octahedron. The Mn2 site should be occupied by Mn^{4+} cations without strong Jahn−Teller distortions of the $Mn2O_6$ octahedron. We note that BVS parameters for Mn^{3+} at B sites of perovskites (for example, in $RMnO_3$ with strong Jahn−Teller distortions where Mn definitely has an oxidation state of +3)[22,23] are often higher than expected (for example, +3.15 to +3.25). At 600 K in the $P4_2/nmc$ model, there is one crystallographic site for the B cations. The BVS value of +3.47 was close to the expected average value of +3.5, and the octahedral distortion parameter had an intermediate value of 7.6 × 10^{-4}, reflecting the statistical presence of 50% of Mn^{3+} cations. Therefore, we conclude that a charge-order (CO) structure is realized below T_{CO} = 425 K. Figure 5 shows temperature dependence of the Mn−O, Cu−O, and Zn−O bond lengths. The Mn1−O1 bond shows a tendency for a gradual decrease with increasing temperature, and the Mn2−O1 and Mn−O1 bonds show a tendency for a gradual increase. Other bonds were nearly temperature independent within the sensitivity of the structural analysis based on synchrotron powder X-ray diffraction.

No DSC anomalies were detected near T_{CO} = 425 K (Figure S2 of the Supporting Information). The temperature dependence of the unit cell volume (Figure 3b) shows no anomalies between 100 and 800 K. The orthorhombic a_O and b_O lattice parameters merge gradually when approaching T_{CO} = 425 K. All of these observations suggest that the structural phase transition at T_{CO} = 425 K is of the second order.

The orthorhombic a_O and b_O lattice parameters and tetragonal a_T lattice parameter monotonically increase with temperature from 100 to 800 K (Figure 3). On the other hand, the orthorhombic c_O lattice parameter slightly increases from 100 to 280 K and then decreases from 280 to 800 K (as c_T above 425 K). Therefore, $Dy_2CuZnMn_4O_{12}$ demonstrates anisotropic thermal expansion above 280 K. As shown in Figure 5, no detectable anomalies were observed on temperature dependence of the bond lengths. Therefore, the origin of the anisotropic thermal expansion is not clear at the moment. Neutron diffraction studies, which can locate oxygen atoms more accurately, will be needed to understand the structural evolution of $Dy_2CuZnMn_4O_{12}$ with temperature more precisely.

Temperature-driven structural phase transitions in $A_2A'A''B_4O_{12}$ perovskites have only been discovered so far in $CaMnTi_2O_6$[7] and $CaMnTi_{2-x}V_xO_6$[8] during a ferroelectric-paraelectric phase transition ($P4_2mc \Leftrightarrow P4_2/nmc$). The discovery of a charge-order transition in $Dy_2CuZnMn_4O_{12}$ ($Pmmn \Leftrightarrow P4_2/nmc$) could suggest the existence of such temperature-driven transitions in other $A_2A'A''B_4O_{12}$ perovskites that crystallize in space group *Pmmn* at room temperature (e.g., RMn_3O_6[10,11] and $R_2CuMnMn_4O_{12}$).[12] High-temperature DSC experiments were performed in the case of RMn_3O_6,[10] but no anomalies were detected. Therefore, it was concluded that RMn_3O_6 does not show charge-order transitions up to 873 K. Our current results give evidence that such transitions could not be detected by DSC, and direct high-temperature structural studies are needed to discover such transitions.

FCC magnetic susceptibilities showed sharp rises below T_C = 116 K in a small applied magnetic field of 100 Oe, suggesting the development of a strong ferromagnetic (FM) component (Figure 6) with additional, gradual rises below about 45 K. The additional anomalies could be more clearly seen on the ZFC curve and on the differential dχT/dT versus T curves (Figure S3). At H = 100 Oe, a difference between the ZFC and FCC χ versus T curves was observed below T_C. At H = 10 kOe, almost

https://doi.org/10.1021/acs.inorgchem.3c02835
Inorg. Chem. 2023, 62, 20042−20049

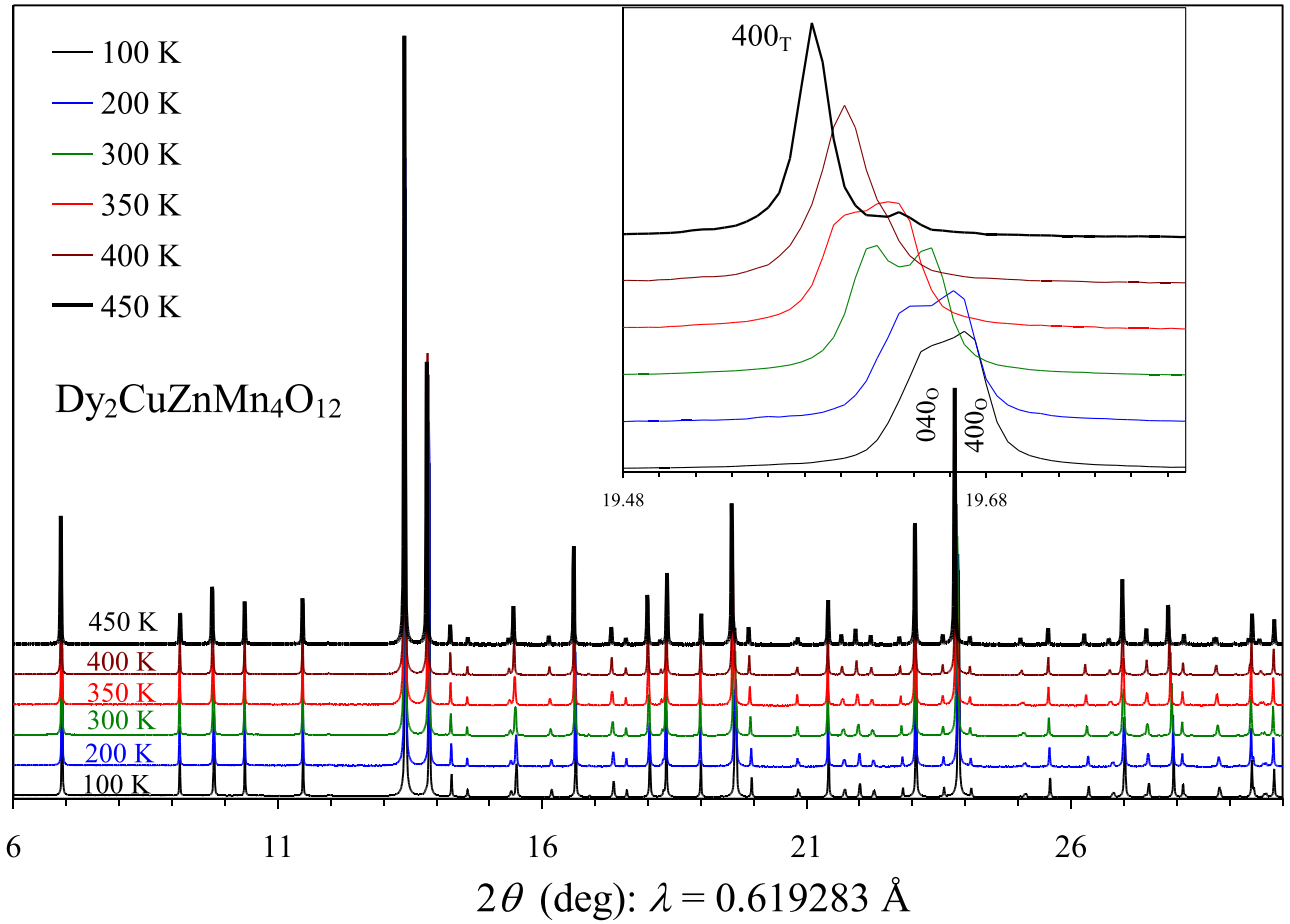

Figure 4. Temperature dependence of the synchrotron X-ray powder diffraction patterns of $Dy_2CuZnMn_4O_{12}$ from 100 to 450 K (between 6 and 30°). The inset shows details near the 040_O, 400_O, and 400_T reflections to emphasize the disappearance of the orthorhombic (O) distortion. T, tetragonal.

Table 3. Structure Parameters of $Dy_2CuZnMn_4O_{12}$ at 600 K from Synchrotron X-ray Powder Diffraction Data[a]

atom	WP	*g*	*x*	*y*	*z*	B_{iso} (Å^2)
Dy	4*d*	1	0.25	0.25	0.22151(5)	0.788(8)
Cu	4*c*	0.5	0.75	0.25	0.7642(8)	1.04(7)
Zn	2*b*	1	0.75	0.25	0.25	0.83(5)
Mn	8*e*	1	0	0	0	0.500(10)
O1	8*g*	1	0.25	0.0629(5)	−0.0362(5)	0.68(7)
O2	8*g*	1	0.25	0.5393(5)	0.5849(5)	1.08(9)
O3	8*f*	1	0.4395(4)	−*x*	0.25	1.51(9)

[a]*g* is the occupation factor. Source: Synchrotron powder X-ray diffraction (λ = 0.61928 Å); used *d*-space range: from 0.4916 to 7.1 Å. Crystal system: tetragonal; space group: $P4_2/nmc$ (no. 137, origin choice 2); Z = 2. Molecular weight: 865.6708 g/mol. a = 7.30342(1) Å, c = 7.75007(2) Å, and V = 413.3886(12) Å^3; R_{wp} = 7.26%, R_p = 5.40%, R_B = 4.78%, and R_F = 3.97%; ρ_{cal} = 6.955 g/cm^3.

Table 4. Bond Lengths (in Å; Below 2.8 Å), Bond Angles (in deg), Bond-Valence Sum (BVS), and Distortion Parameters of MnO_6 (Δ) in $Dy_2CuZnMn_4O_{12}$ at 600 K[a]

Dy−O1 × 2	2.323(4)	Mn−O1 × 2	1.904(1)
Dy−O2 × 2	2.363(4)	Mn−O2 × 2	1.962(2)
Dy−O1 × 2	2.420(4)	Mn−O3 × 2	2.036(1)
Dy−O3 × 4	2.666(1)	$\Delta(MnO_6)$	7.6×10^{-4}
BVS(Dy^{3+})	+3.19	BVS(Mn^{3+})	+3.47
Cu−O3 × 4	1.960(4)	Mn−O1−Mn × 2	147.15(6)
BVS(Cu^{2+})	+1.87	Mn−O2−Mn × 2	137.08(6)
Zn−O2 × 4	2.002(4)	Mn−O3−Mn × 2	144.25(6)
BVS(Zn^{2+})	+1.79		

no difference was detected between the ZFC and FCC χ versus T curves. The χ^{-1} versus T curves followed the Curie−Weiss law, and a fit by the law between 300 and 400 K gave a positive Curie−Weiss temperature, θ = +125 K, indicating predominantly FM interactions between magnetic ions. The calculated effective magnetic moment (μ_{calc}) is 17.485μ_B (for the calculation we used 10.6μ_B for Dy^{3+}, 4.899μ_B for Mn^{3+}, 3.873μ_B for Mn^{4+}, and 1.732μ_B for Cu^{2+} and an equation $\mu_{calc}{}^2 = 2\,\mu_{Dy}{}^2 + 2\,\mu_{Mn(III)}{}^2 + 2\,\mu_{Mn(IV)}{}^2 + \mu_{Cu}{}^2$). The experimental effective magnetic moment was about 9% smaller (μ_{eff} = 15.99μ_B). While the origin of this reduction is not clear at the moment, the same tendency was observed for all other members

https://doi.org/10.1021/acs.inorgchem.3c02835
Inorg. Chem. 2023, 62, 20042−20049

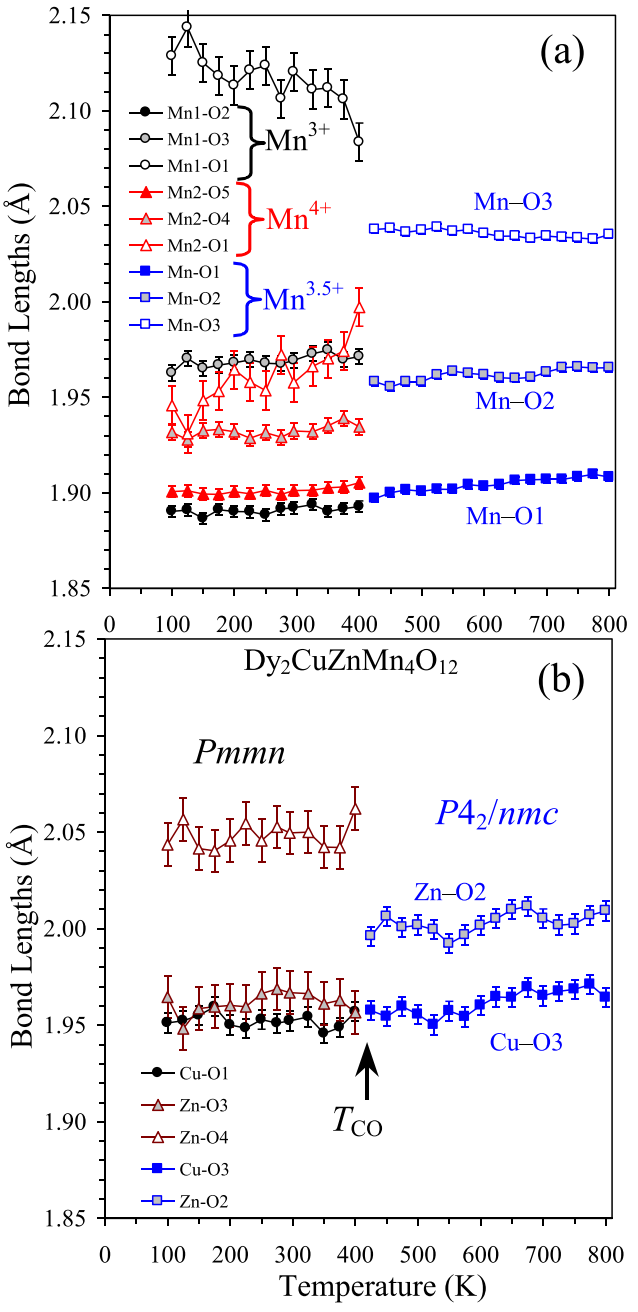

Figure 5. Temperature dependence of (a) the Mn−O bond lengths and (b) the Cu−O and Zn−O bond lengths in $Dy_2CuZnMn_4O_{12}$.

of the $R_2CuZnMn_4O_{12}$ (for example, $\mu_{calc} = 9.00\mu_B$ versus $\mu_{eff} = 8.29\mu_B$ for R = Lu) and $R_2CuGaMn_4O_{12}$ series.[3]

Temperature dependence of magnetic susceptibilities of $Dy_2CuZnMn_4O_{12}$ was qualitatively similar to that of the parent $Dy_2MnMnMn_4O_{12}$ (= $DyMn_3O_6$).[10] But the absolute values of magnetic susceptibilities were about 10 times larger in $Dy_2CuZnMn_4O_{12}$ at both H = 100 Oe and 10 kOe. This fact suggests that the ordered moments in $Dy_2CuZnMn_4O_{12}$ were much larger than those of $Dy_2MnMnMn_4O_{12}$. Recent neutron diffraction studies found that the ordered moments were significantly reduced (in comparison with the expected full moments) in an isostructural compound $Y_2MnMnMn_4O_{12}$ due to competing exchange interactions, and there was a competition between antiferromagnetic and ferrimagnetic ground states.[24] The magnetic frustration could be reduced through the introduction of nonmagnetic Zn^{2+} cations into the A″ site in $Dy_2CuZnMn_4O_{12}$ and through the full charge ordering of Mn^{3+} and Mn^{4+}, resulting in larger ordered magnetic moments. The gradual rise of magnetic susceptibilities below 45 K could be caused by the gradual increase of the ordered moments of the Dy^{3+} sublattices, but it was difficult (from the available data) to determine at what temperature the Dy^{3+} sublattices start to order.

On the other hand, temperature dependence of magnetic susceptibilities of $Dy_2CuZnMn_4O_{12}$ was different from that of $Dy_2CuMnMn_4O_{12}$ at small magnetic fields and at temperatures below about 40 K.[12] In $Dy_2CuMnMn_4O_{12}$, magnetic susceptibilities decreased at low temperatures. This fact suggests different magnetic structures for these two compounds. The magnetic susceptibility behavior of $Dy_2CuMnMn_4O_{12}$ was consistent with the determined magnetic structure, where the Dy1 and Dy2 sublattices order antiferromagnetically relative to each other but with different magnitudes, and the resulting uncompensated moment on the Dy sublattices aligns antiferromagnetically relative to the FM Mn sublattices.[12]

Isothermal magnetization measurements (Figure 7) showed a behavior typical for soft ferrimagnets with a coercive field, H_C, of about 200 Oe at T = 5 K and a large saturation magnetization, M_S, of about $25.6\mu_B$ (at T = 5 K and H = 70 kOe). The near saturation value was already observed from about H = 20 kOe. This saturation value is smaller than the full magnetization of $35\mu_B$ expected for a full FM alignment (using the maximum value of 10 μ_B for Dy^{3+}). On the other hand, Dy^{3+} cations have a noticeable single-ion anisotropy; therefore, the full moment of Dy^{3+} cannot be reached in powder samples. Magnetic structures of related compounds, $Dy_2CuMnMn_4O_{12}$ and $Y_2CuGaMn_4O_{12}$, were investigated by neutron diffraction. It was found that the B-site Mn sublattices are ordered ferromagnetically but with reduced magnetic moments ($2.2\mu_B$ per Mn in $Y_2CuGaMn_4O_{12}$ and $2.5\mu_B$ per Mn^{4+} and $3.3\mu_B$ per Mn^{3+} in $Dy_2CuMnMn_4O_{12}$). Considering uncertainties in ordered moments on the Dy and Mn sublattices, the maximum contribution of $1\mu_B$ from the Cu sublattice of $Dy_2CuZnMn_4O_{12}$ can be neglected in the discussion below.

M_S was about $9.5\mu_B$ (at T = 5 K) in a related compound without magnetic rare-earth cations, $Lu_2CuZnMn_4O_{12}$ (the inset of Figure 7), given an average moment of $2.4\mu_B$ per Mn, which is close to the experimentally determined values in the related compounds. Assuming a similar magnetic structure with similar ordered moments at the B sublattices in $Dy_2CuZnMn_4O_{12}$ and $Lu_2CuZnMn_4O_{12}$, the difference in the M_S values could be attributed to the Dy^{3+} sublattices. The difference was about $16\mu_B$, which was significantly larger than the maximum Dy^{3+} ordered moment. This fact suggests that both Dy^{3+} sublattices (Dy1 and Dy2) give FM contributions to the magnetic structure with an average value of $8\mu_B$. Therefore, M versus H curves of $Dy_2CuZnMn_4O_{12}$ (and comparison with the related compounds) suggest that the Mn1 and Mn2 sublattices are ordered ferromagnetically and the Dy1 and Dy2 sublattices are ordered ferromagnetically relative to each other and to the Mn sublattices.

4. CONCLUSIONS

In conclusion, we prepared a new member of the A-site columnar-ordered quadruple perovskites, $Dy_2CuZnMn_4O_{12}$, which crystallizes in the charge-order structure at room temperature with *Pmmn* symmetry. Using direct high-temper-

https://doi.org/10.1021/acs.inorgchem.3c02835
Inorg. Chem. 2023, 62, 20042−20049

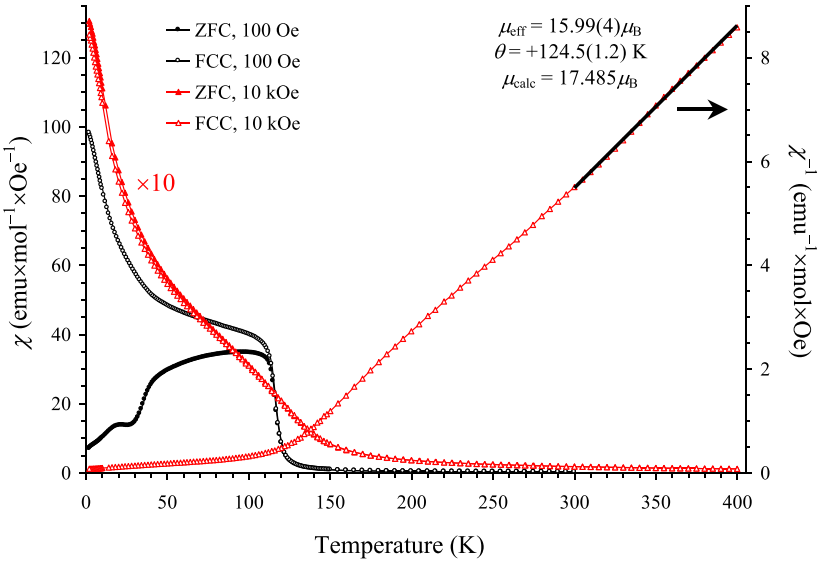

Figure 6. Left-hand axis presents ZFC (filled symbols) and FCC (empty symbols) dc magnetic susceptibility ($\chi = M/H$) curves of $Dy_2CuZnMn_4O_{12}$ measured at 100 Oe and 10 kOe (multiplied by 10). Right-hand axis shows the FCC χ^{-1} versus T curves at 10 kOe with the Curie–Weiss fit (black line). Parameters of the fit are shown on the figure.

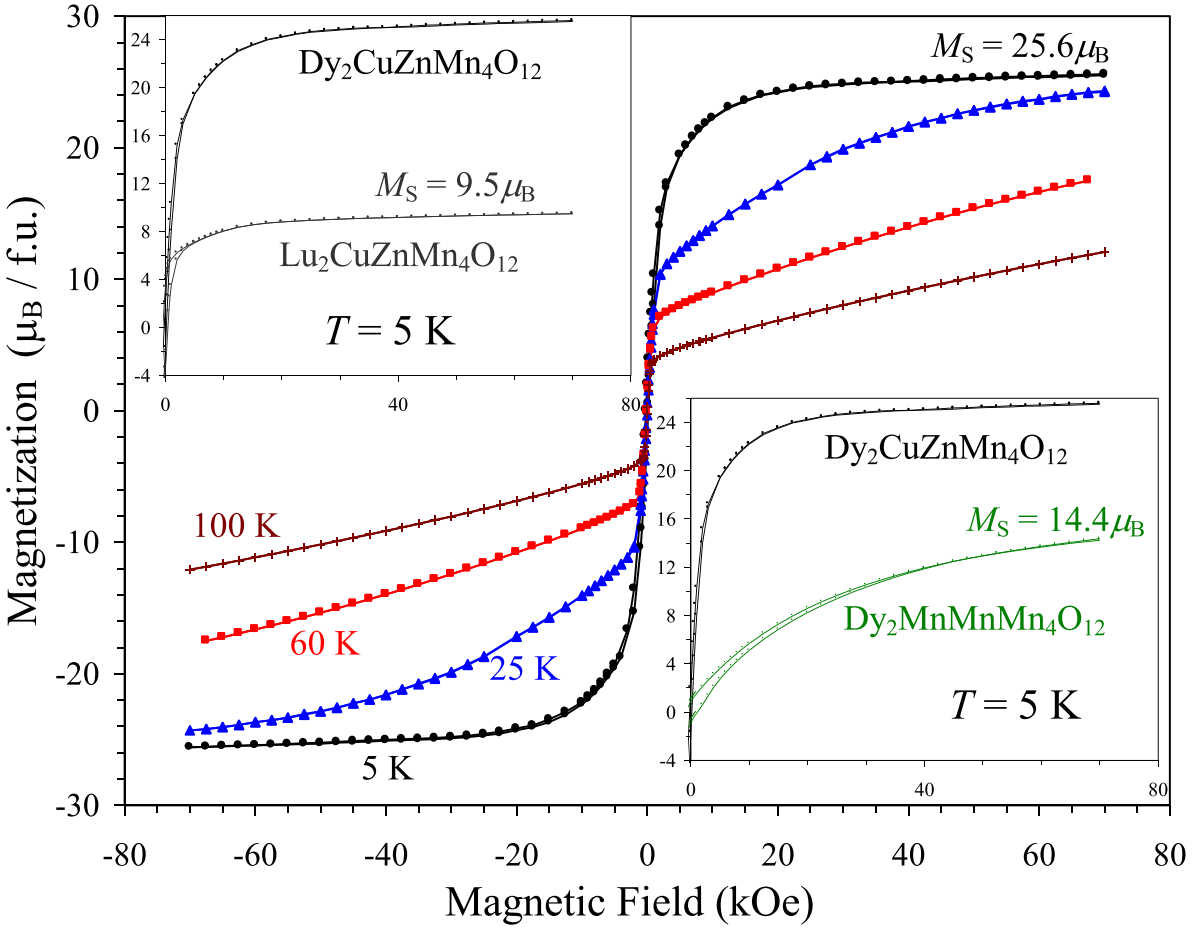

Figure 7. M versus H curves of $Dy_2CuZnMn_4O_{12}$ at 5, 25, 60, and 100 K (f.u.: formula unit). The left-hand inset compares M versus H curves of $Dy_2CuZnMn_4O_{12}$ and $Lu_2CuZnMn_4O_{12}$ at 5 K. The right-hand inset compares M versus H curves of $Dy_2CuZnMn_4O_{12}$ and $Dy_2MnMnMn_4O_{12}$[10] at 5 K. M_S is the magnetization value at H = 70 kOe and T = 5 K.

ature structural studies, we could detect a charge-disorder transition above 425 K, while other methods could not detect such a transition. Triple A-site cation ordering was realized through a new combination of the A/A′/A″ cations (Dy^{3+}/Cu^{2+}/Zn^{2+}). $Dy_2CuZnMn_4O_{12}$ exhibits a ferrimagnetic tran-

https://doi.org/10.1021/acs.inorgchem.3c02835
Inorg. Chem. 2023, 62, 20042−20049

sition below 116 K with a large saturation magnetization and involvement of the Dy^{3+} sublattices at low temperatures.

■ ASSOCIATED CONTENT

Supporting Information

The Supporting Information is available free of charge at https://pubs.acs.org/doi/10.1021/acs.inorgchem.3c02835.

Bond distances of $Dy_2CuZnMn_4O_{12}$ at 100 K, DSC curves, details of M vs H curves, M vs T curves, and differential magnetic susceptibility curves, ac magnetic susceptibility curves, and a photograph of the as-synthesized powder (PDF)

■ AUTHOR INFORMATION

Corresponding Author

Alexei A. Belik − *Research Center for Materials Nanoarchitectonics (MANA), National Institute for Materials Science (NIMS), Tsukuba, Ibaraki 305-0044, Japan;* orcid.org/0000-0001-9031-2355; Email: Alexei.Belik@nims.go.jp

Complete contact information is available at: https://pubs.acs.org/10.1021/acs.inorgchem.3c02835

Notes

The author declares no competing financial interest.

■ ACKNOWLEDGMENTS

The synchrotron radiation experiments were performed at SPring-8 with the approval of Japan Synchrotron Radiation Research Institute (proposal numbers: 2023A1496 and 2023A2361). We thank Dr. S. Kobayashi for his help at BL02B2 of SPring-8.

■ REFERENCES

(1) Belik, A. A. Rise of A-site Columnar-Ordered $A_2A'A''B_4O_{12}$ Quadruple Perovskites with Intrinsic Triple Order. *Dalton Trans.* **2018**, *47*, 3209−3217.

(2) Liu, R.; Khalyavin, D. D.; Tsunoda, N.; Kumagai, Y.; Oba, F.; Katsuya, Y.; Tanaka, M.; Yamaura, K.; Belik, A. A. Spin-Glass Magnetic Properties of A-Site Columnar-Ordered Quadruple Perovskites $Y_2MnGa(Mn_{4-x}Ga_x)O_{12}$ with $0 \leq x \leq 3$. *Inorg. Chem.* **2019**, *58*, 14830−14841.

(3) Belik, A. A.; Khalyavin, D. D.; Matsushita, Y.; Yamaura, K. Triple A-site Cation Ordering in the Ferrimagnetic $Y_2CuGaMn_4O_{12}$ Perovskite. *Inorg. Chem.* **2022**, *61*, 14428−14435.

(4) Belik, A. A.; Liu, R.; Yamaura, K. Spin-glass to Long-range Order to Spin-glass Evolution of Magnetic Properties with the Composition in $Sm_2MnZnMn_{4-x}Ti_xO_{12}$ (x = 1, 2, and 3) Perovskites. *J. Alloys Compd.* **2023**, *932*, No. 167727.

(5) Belik, A. A.; Liu, R.; Yamaura, K. Realization of Triple A-site Cation Ordering through the Dy/Mn/Zn Combination in the Ferrimagnetic $Dy_2MnZnMn_{4-x}Ti_xO_{12}$ Perovskites. *Ceram. Int.* **2023**, *49*, 14327−14334.

(6) Azuma, M.; Yamada, I.; Yamaura, K.; Belik, A. A.; Yamamoto, T.; Fukuda, M. 4.20 - High Pressure Studies of Transition Metal Oxides. In *Comprehensive Inorganic Chemistry III*, 3rd ed.; Reedijk, J., Poeppelmeier, K. R., Eds.; Elsevier: Oxford, 2023; pp 681−718. DOI: 10.1016/B978-0-12-823144-9.00141-2.

(7) Aimi, A.; Mori, D.; Hiraki, K.; Takahashi, T.; Shan, Y. J.; Shirako, Y.; Zhou, J. S.; Inaguma, Y. High-Pressure Synthesis of A-site Ordered Double Perovskite $CaMnTi_2O_6$ and Ferroelectricity Driven by Coupling of A-site Ordering and the Second-order Jahn−Teller Effect. *Chem. Mater.* **2014**, *26*, 2601−2608.

(8) Fukuda, M.; Nishikubo, T.; Pan, Z.; Sakai, Y.; Zhang, M.-H.; Kawaguchi, S.; Yu, H.; Okimoto, Y.; Koshihara, S.-Y.; Itoh, M.; Rödel, J.; Azuma, M. Enhanced Spontaneous Polarization by V^{4+} Substitution in a Lead-Free Perovskite $CaMnTi_2O_6$. *Inorg. Chem.* **2020**, *59*, 11749−11756.

(9) Scatena, R.; Liu, R.; Shvartsman, V. V.; Khalyavin, D. D.; Inaguma, Y.; Yamaura, K.; Belik, A. A.; Johnson, R. D. Hybrid Improper Ferroelectricity in Columnar (NaY)$MnMnTi_4O_{12}$. *Angew. Chem., Int. Ed.* **2023**, *62*, No. e202305994.

(10) Zhang, L.; Matsushita, Y.; Yamaura, K.; Belik, A. A. Five-fold Ordering in High-pressure Provskites RMn_3O_6 (R = Gd-Tm and Y). *Inorg. Chem.* **2017**, *56*, 5210−5218.

(11) Belik, A. A.; Zhang, L.; Matsushita, Y.; Katsuya, Y.; Tanaka, M.; Yamaura, K. Crystal Structures of Cation Non-stoichiometric RMn_3O_6 (R = Gd, Er, and Tm) Manganites Belonging to A-site Columnar-ordered Quadruple Perovskite Family. *J. Solid State Chem.* **2019**, *275*, 43−48.

(12) Vibhakar, A. M.; Khalyavin, D. D.; Manuel, P.; Liu, J.; Belik, A. A.; Johnson, R. D. Spontaneous Rotation of Ferrimagnetism Driven by Antiferromagnetic Spin Canting. *Phys. Rev. Lett.* **2020**, *124*, No. 127201.

(13) Salamon, M. B.; Jaime, M. The Physics of Magnanites: Structure and Transport. *Rev. Mod. Phys.* **2001**, *73*, 583−628.

(14) Yamada, I. High-pressure Synthesis, Electronic States, and Structure-property Relationships of Perovskite Oxides, $ACu_3Fe_4O_{12}$ (A: Divalent Alkaline Earth or Trivalent Rare-earth Ion). *J. Ceram. Soc. Jpn.* **2014**, *122*, 846−851.

(15) Decker, D. L.; Vanfleet, H. B. Melting and High-temperature Electrical Resistance of Gold under Pressure. *Phys. Rev.* **1965**, *138*, A129−A133.

(16) Kawaguchi, S.; Takemoto, M.; Osaka, K.; Nishibori, E.; Moriyoshi, C.; Kubota, Y.; Kuroiwa, Y.; Sugimoto, K. High-throughput Powder Diffraction Measurement System Consisting of Multiple MYTHEN Detectors at Beamline BL02B2 of SPring-8. *Rev. Sci. Instrum.* **2017**, *88*, No. 085111.

(17) Izumi, F.; Ikeda, T. A Rietveld-analysis Program RIETAN-98 and its Applications to Zeolites. *Mater. Sci. Forum* **2000**, *321*−*324*, 198−205.

(18) Waroquiers, D.; Gonze, X.; Rignanese, G.-M; Welker-Nieuwoudt, C.; Rosowski, F.; Göbel, M.; Schenk, S.; Degelmann, P.; André, R.; Glaum, R.; Hautier, G. Statistical Analysis of Coordination Environments in Oxides. *Chem. Mater.* **2017**, *29*, 8346−8360.

(19) Fukuda, M.; Nishikubo, T.; Yu, H. W.; Okimoto, Y.; Koshihara, S.-Y.; Yamaura, K.; Azuma, M. A-Site Columnar-Ordered Perovskite $CaZnV_2O_6$ as a Pauli-Paramagnetic Metal. *Inorg. Chem.* **2023**, *62*, 8372−8378.

(20) Solana-Madruga, E.; Kearins, P. S.; Ritter, C.; Arévalo-López, Á. M.; Attfield, J. P. 1:1 Ca^{2+}:Cu^{2+} A-site Order in a Ferrimagnetic Double Double Perovskite. *Angew. Chem., Int. Ed.* **2022**, *61*, No. e202209497.

(21) Brese, N. E.; O'Keeffe, M. Bond-valence Parameters for Solids. *Acta Crystallogr., Sect. B: Struct. Sci.* **1991**, *47*, 192−197.

(22) Alonso, J. A.; Martinez-Lope, M. J.; Casais, M. T.; Fernandez-Diaz, M. T. Evolution of the Jahn-Teller Distortion of MnO_6 Octahedra in $RMnO_3$ Perovskites (R = Pr, Nd, Dy, Tb, Ho, Er, Y): A Neutron Diffraction Study. *Inorg. Chem.* **2000**, *39*, 917−923.

(23) Tachibana, M.; Shimoyama, T.; Kawaji, H.; Atake, T.; Takayama-Muromachi, E. Jahn-Teller Distortion and Magnetic Transitions in Perovskite $RMnO_3$ (R = Ho, Er, Tm, Yb, and Lu). *Phys. Rev. B: Condens. Matter Mater. Phys.* **2007**, *75*, No. 144425.

(24) Vibhakar, A. M.; Khalyavin, D. D.; Manuel, P.; Steinke, N. J.; Zhang, L.; Yamaura, K.; Belik, A. A.; Johnson, R. D. Magnetic Inhomogeneities in the Quadruple Perovskite Manganite $[Y_{2-x}Mn_x]Mn_6O_{12}$. *Phys. Rev. B: Condens. Matter Mater. Phys.* **2023**, *108*, No. 054403.